Article

Preparation of Manganese Blending-Modified Activated Coke for Flue Gas Desulfurization

Wenjie Liao, Xiaomi Meng, Lu Yao, Wenju Jiang, and Lin Yang*

Read Online

ACCESS | Metrics & More | Article Recommendations

ABSTRACT: In this study, the preparation and desulfurization application of MnO_2 and pyrolusite blending-modified activated cokes (ACM and ACP) were studied. Thermodynamic calculation shows that the blended metal oxides could be reacted with the solid carbon and gaseous products H_2, CO, and CO_2 for activation. The physicochemical properties of the blending-modified ACP and ACM responded considerably differently to preparation conditions. The blended metal oxide significantly improved the mesoporous structure of the modified activated cokes, as well as the surface acidic and basic functional groups. Different metal oxides played different roles in the pore structure and surface functional group evolution, and the current investigation indicates that MnO_2 is more favorable than pyrolusite. The enhanced acidic and basic functional groups, coupled with the catalysis of metal oxides, improved the desulfurization performance of the modified activated cokes. The sulfur capacities of the prepared ACP and ACM were 47.9−208.9 and 119.4−205.9 mg/g, respectively, which were much greater than the sulfur capacity of the fresh activated coke.
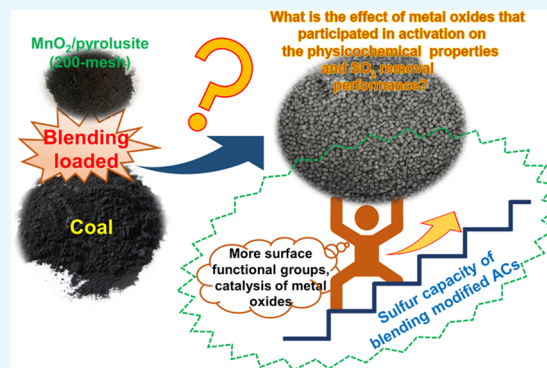
1. INTRODUCTION

Carbonaceous materials such as activated carbon/coke (AC), activated carbon fiber, and carbon nanotube are frequently employed in almost every area of our life.[1−5] Among them, activated coke is one of the most promising materials in environmental applications such as desulfurization,[6] denitrification,[7] and air toxic removal[8] due to the wide availability of its raw materials, low preparation cost, and high mechanical strength.[9]

Because of the relative bad activity of the conventional AC, surface modification, including heat treatment,[10,11] heteroatom doping,[12,13] and loading some kind of transition metal oxides,[10,13,14] is widely used now. The introduction of metal oxide to make traditional AC to adsorbent-catalyst is the most extensively used method in the field of flue gas desulfurization and denitrification. The most commonly used method of metal oxide loading is the impregnation method, which is typically a post-treatment method and includes three steps, acidic treatment, chemical deposition, and calcination. It is characterized by a complicated procedure, is costly, and is always followed by secondary pollution.[15−17] Furthermore, in most cases, the liquid−solid two-phase mass transfer restricts ion diffusion of the internal pore structure, and the dispersion of the loaded metal particles is poor, for example, V_2O_5-species tend to finish in egg shells in AC body.[18−20]

The blending modification, however, is fundamentally different. The solid powder precursor is directly mixed with raw carbon materials in solid and then the material is run through kneading, modeling, carbonization, and activation as a whole preparation process to obtain the modified AC product.[21] It is a one-step preparation and modification method where the introduced transition metal could distribute uniformly throughout the carbon matrix and participate in the carbonization−activation process.[22] Therefore, the reactions of the blending modified ACs are more complicated than that of the conventional ACs. The blended metal oxide likewise reacts to the carbon and activation byproducts but does not react to the conventional oxidation and pyrolysis. In addition, pyrolysis processes may also be differed in the presence of the catalytic activity of metal oxide. These distinctions induced by the blending-introduced metal oxides lead to the surface chemical and porosity heterogeneity of AC.[23,24]

Some researchers have studied the blending modification of AC with different types of metal oxides in previous work.[25−27] Natural minerals, such as titanium ore and pyrolusite, were used as additives for the modification of AC.[28,29] The influence of three types of pyrolusite blending and two different activators (CO_2 and water steam) on the AC products have

been studied,[30] which revealed that AC blended with different types of pyrolusite showed clear diversity in physicochemical properties. However, all the earlier papers on the blending modification are focused on the modifier type and load ratio. The deep understanding of the influences of the blending modification on the preparation of AC carbon is still not clear, and the controlled preparation of the blending modified AC is in progress.

In this work, the nonmodified AC and the MnO_2 and pyrolusite blending-modified ACM and ACP were prepared by water steam activation in order to investigate the responses of blending modification by different additives to the key preparation conditions including activation temperature, activation time, and the amount of activator. The burn off (BO) that directly corresponded to the preparation cost, the iodine number and N_2 adsorption−desorption that identified the porosity, and the total surface acidic and basic functional groups that related to the potential desulfurization performance were chosen as the evaluation index to explore the conceivable responsibilities. After that, the simulated flue gas desulfurization test of all the prepared samples were carried out to verify the final influences of blending modification on its SO_2 removal performance.

2. RESULTS AND DISCUSSION

2.1. Thermodynamic Calculation. Commonly, the main reaction of the steam activation of AC happened between the carbon and water steam (eq 1 in Table 1), which formed much of the content of new pore of coke and connected the pore structure created by carbonization.[31] After being blended with MnO_2 or pyrolusite, the reactions between metal oxides (manganese and iron oxides) and solid carbon or the conventional gaseous products H_2, CO, and CO_2 also took place because of the strong reduction condition and high temperature (>800 °C).[32] The previous study revealed that MnO_2 and Fe_2O_3 were reduced to MnO, FeO, and Fe^0. Therefore, the thermodynamics calculation between metal oxides and carbon or gaseous products at 800 °C was carried out using FactSage software (FactSage 7.1). It can be seen that the $\Delta_r G_m$ of the listed reactions are negative at the lowest activation temperature of 800 °C, indicating that the steam activation is a forward reaction at all four selected activation temperatures. The eqs 2−13 in Table 1 indicate that MnO_2 could be reduced to form MnO directly by the reductants such as carbon, H_2, and CO (eqs 6, 7, 10, and 13 in Table 1) or reacted with them to form Mn_2O_3 and Mn_3O_4 step by step, and finally reduced to MnO (eqs 2−13 in Table 1). The calculations indicate that there may be up to four chemical states of manganese oxide on the surface of the blended activated coke. However, as shown in Figure 1, only MnO_2 and MnO was detected on the surface of AC, which means the reduction of MnO_2 is exhaustive, and no intermediate (i.e., Mn_2O_3 and Mn_3O_4) is reserved, and this result is consistent with the previous study.[28,33] Due to the co-existence of Fe_2O_3 in pyrolusite, the reactions of Fe_2O_3 in the activation process were also considered. The eqs 14−30 in Table 1 show that the reduction of Fe_2O_3 to FeO could be also completed. The X-ray diffraction (XRD) analysis of ACP-1/1-800-60 shows that there was no Fe_3O_4 detected (Figure 1), indicating that the intermediate state of Fe_3O_4 is unstable in the blending modified ACP.

The thermodynamics calculations presented the complication well of the activation system of metal-modified AC. On

Table 1. $\Delta_r G_m$ of the Potential Reactions that Occurred at 800 °C during the Steam Activation of the Modified AC

reactions	$\Delta_r G_m$ (kJ/mol)	eqs
$H_2O_{(g)} + C_{(s)} = H_{2(g)} + CO_{(g)}$	−18.063	1
$2MnO_{2(s)} + C_{(s)} = Mn_2O_{3(s)} + CO_{(g)}$	−243.421	2
$4MnO_{2(s)} + C_{(s)} = 2Mn_2O_{3(s)} + CO_{2(g)}$	−469.615	3
$3MnO_{2(s)} + 2C_{(s)} = Mn_3O_{4(s)} + 2CO_{(g)}$	−454.310	4
$3MnO_{2(s)} + C_{(s)} = Mn_3O_{4(s)} + CO_{2(g)}$	−437.082	5
$MnO_{2(s)} + C_{(s)} = MnO_{(s)} + CO_{(g)}$	−188.583	6
$2MnO_{2(s)} + C_{(s)} = 2MnO_{(s)} + CO_{2(g)}$	−359.940	7
$MnO_{2(s)} + H_{2(g)} = Mn_2O_{3(s)} + H_2O_{(g)}$	−225.358	8
$MnO_{2(s)} + H_{2(g)} = Mn_3O_{4(s)} + H_2O_{(g)}$	−418.183	9
$MnO_{2(s)} + H_{2(g)} = MnO_{(s)} + H_2O_{(g)}$	−170.520	10
$MnO_{2(s)} + CO_{(g)} = Mn_2O_{3(s)} + CO_{2(g)}$	−226.193	11
$MnO_{2(s)} + CO_{(g)} = Mn_3O_{4(s)} + CO_{2(g)}$	−419.854	12
$MnO_{2(s)} + CO_{(g)} = MnO_{(s)} + CO_{2(g)}$	−171.356	13
$3Fe_2O_{3(s)} + C_{(s)} = 2Fe_3O_{4(s)} + CO_{(g)}$	−109.501	14
$6Fe_2O_{3(s)} + C_{(s)} = 4Fe_3O_{4(s)} + CO_{2(g)}$	−201.776	15
$Fe_2O_{3(s)} + C_{(s)} = 2FeO_{(s)} + CO_{(g)}$	−51.900	16
$2Fe_2O_{3(s)} + C_{(s)} = 4FeO_{(s)} + CO_{2(g)}$	−86.574	17
$Fe_3O_{4(s)} + C_{(s)} = 3FeO_{(s)} + CO_{(g)}$	−23.100	18
$2Fe_3O_{4(s)} + C_{(s)} = 6FeO_{(s)} + CO_{2(g)}$	−28.973	19
$Fe_3O_{4(s)} + 4C = Fe_{(s)} + 4CO_{(g)}$	−57.583	20
$Fe_3O_{4(s)} + 2C = 3Fe_{(s)} + 2CO_{2(g)}$	−23.128	21
$FeO_{(s)} + C_{(s)} = Fe_{(s)} + CO_{(g)}$	−560.530	22
$3Fe_2O_3 + H_{2(g)} = 2Fe_3O_4 + H_2O_{(g)}$	−91.438	23
$Fe_2O_{3(s)} + H_{2(g)} = 2FeO_{(s)} + H_2O_{(g)}$	−33.837	24
$Fe_2O_{3(s)} + 3H_{2(g)} = 2Fe_{(s)} + 3H_2O_{(g)}$	−20.700	25
$Fe_3O_{4(s)} + H_{2(g)} = 3FeO + H_2O_{(g)}$	−5.037	26
$3Fe_2O_{3(s)} + CO_{(g)} = 2Fe_3O_{4(s)} + CO_{2(g)}$	−92.274	27
$Fe_2O_{3(s)} + CO_{(g)} = 2FeO_{(s)} + CO_{2(g)}$	−34.673	28
$Fe_3O_{4(s)} + CO_{(g)} = 3FeO_{(s)} + CO_{2(g)}$	−5.872	29
$Fe_2O_{3(s)} + 3CO_{(g)} = 2Fe_{(s)} + 3CO_{2(g)}$	−23.206	30
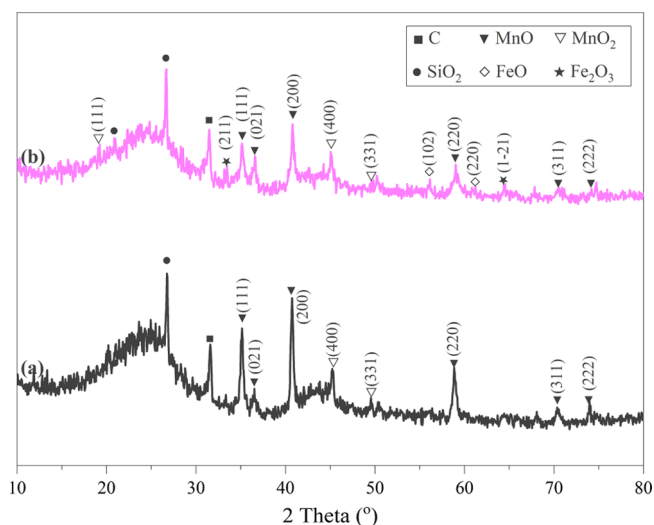
Figure 1. XRD patterns of ACM-1/1-800-60 (a) and ACP-1/1-800-60 (b).

the one hand, the reduction of metal oxides should be different. On the other hand, the metal oxides participating in the carbonization and activation processes should also affect the evolution of pore structure and surface chemical properties of AC due to its catalytic activity. Therefore, the influences of these new reactions in the physicochemical properties of modified AC should be seriously discussed.
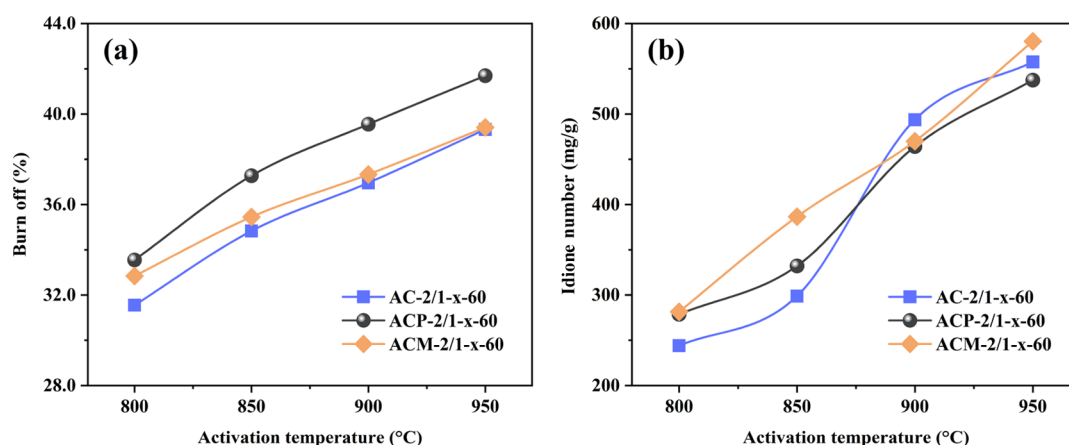
Figure 2. BO (a) and iodine number (b) of ACs prepared under different activation temperatures.

2.2. Influences of Activation Temperature.

2.2.1. BO and Iodine Number of ACs.

The BO and iodine number of the activated cokes prepared at different activation temperatures are given in Figure 2. It can be seen that the BO of the fresh AC linearly increased with the increase of activation temperature (Figure 2a). After being blended with MnO_2 and pyrolusite, the BO of ACP and ACM was relatively high as compared with AC except when ACM was prepared at 950 °C, and the BO was also proportional to the activation temperature. ACP had at least 2.00% higher BO than AC (from 2.00 to 2.59%), whereas the BO of ACM tended to be close to that of AC with an increase of the activation temperature, the difference between them reduced from 1.29% at 800 °C to only 0.09% at 950 °C. Lee et al.[34] had reported that the metal particles could promote aggregation performance of carbon to form large crystals, which could restrict the reactions between carbon and reductants to cause a relatively lower BO. The absolute metal content by blending MnO_2 is higher than that by blending pyrolusite with the same blending ratio, so the high temperature aggregation of ACM should be theoretically stronger to limit the BO during activation. The iodine numbers are presented in Figure 2b. The higher activation temperature in the preparation of ACs, the higher the iodine number obtained. The iodine number of ACM and ACP became more linear with the increase of activation temperature than AC, and the pore structure generation is more responsive to the relative lower activation temperature when the metal oxide was blended. ACP and ACM prepared at 800 and 850 °C showed a larger iodine adsorption capacity than AC. However, they were quite close when the activation temperature increased to 900 and 950 °C. Coupled with the variation of BO in the samples showed that the metal oxides blended enhanced the high-temperature agglomeration of the preparation process.

2.2.2. Textual Property of ACs.

Figure 3 shows the N_2 adsorption–desorption isotherms of the samples prepared at different activation temperatures. The prepared ACs exhibited typically type I isotherms with a H4 hysteresis, indicating a uniform microporosity coupled with a certain amount of mesoporous structure.[35,36] The microporosity of ACP and ACM was not visibly changed, while they all showed a relatively stronger N_2 adsorption at a high P/P^0 range (>0.8) and larger hysteresis loop, especially ACM. This indicates that there were more mesoporous structures of ACM and ACP.

The textual properties, including the surface area (S_{BET}), surface area of mesopores (S_{mes}), total pore volume (V_{tot}),
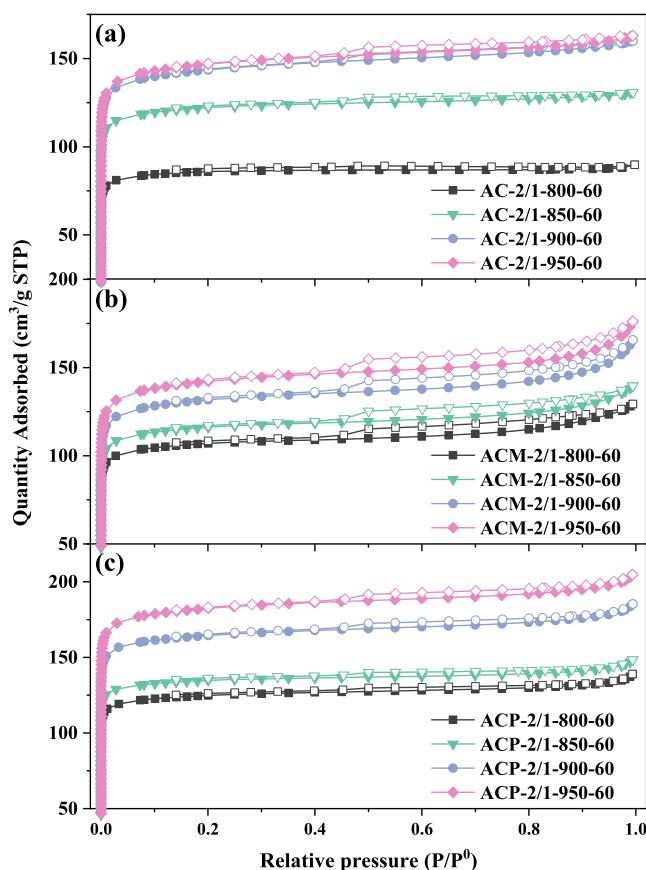
Figure 3. N_2 adsorption–desorption isotherms of ACs prepared under different activation temperatures: (a) AC-, (b) ACM-, and (c) ACP-.

micropore volume (V_{mic}), mesopore volume (V_{mes}), and average pore diameter (DI) of samples, are listed in Table 2. Similar to the changes of the iodine number and BO with increasing activation temperature, the S_{BET} of AC linearly increased with the increase of activation temperature, from 277 m^2/g at 800 °C to 469 m^2/g at 950 °C. However, the improvement of S_{BET} was not clear when the activation temperature was higher than 900 °C. The blending of metal oxides could improve the pore structure of samples at a relatively low activation temperature, whereas its agglomeration at high temperatures is an important inhibition. ACM

Table 2. Porosity Parameters of ACs

parameters		2/1-T_A-60 (°C)				2/1-900-t (min)			a-900-60 <>(M_C/M_{H_2O})<>		
		800	850	900	950	40	80	100	5/1	3/1	1/1
S_{BET} (m²/g)	AC-	272	388	459	469	446	400	413	423	454	511
	ACP-	338	350	402	443	387	425	426	285	385	427
	ACM-	340	370	421	454	423	463	458	363	385	490
S_{mes} (m²/g)	AC-	11.84	26.29	44.55	44.39	15.46	23.32	33.16	32.61	46.90	80.15
	ACP-	20.70	25.67	37.23	43.16	39.96	46.13	46.47	15.31	34.35	43.94
	ACM-	26.26	30.53	40.46	46.07	34.76	65.03	47.2	38.19	19.34	89.33
V_{tot} (cm³/g)	AC-	0.138	0.202	0.247	0.252	0.241	0.205	0.218	0.23	0.255	0.304
	ACP-	0.178	0.193	0.226	0.248	0.217	0.236	0.249	0.155	0.215	0.248
	ACM-	0.199	0.215	0.255	0.272	0.252	0.297	0.284	0.211	0.219	0.339
V_{mic} (cm³/g)	AC-	0.119	0.165	0.187	0.192	0.18	0.172	0.173	0.177	0.184	0.192
	ACP-	0.136	0.137	0.161	0.18	0.156	0.165	0.171	0.123	0.159	0.173
	ACM-	0.144	0.155	0.171	0.183	0.173	0.178	0.186	0.145	0.167	0.178
V_{mes} (cm³/g)	AC-	0.019	0.037	0.06	0.06	0.061	0.033	0.045	0.053	0.071	0.112
	ACP-	0.042	0.056	0.065	0.068	0.061	0.071	0.078	0.032	0.056	0.075
	ACM-	0.055	0.06	0.084	0.089	0.079	0.119	0.098	0.066	0.052	0.161
DI (nm)	AC-	2.03	2.08	2.15	2.15	2.16	2.06	2.11	2.18	2.25	2.38
	ACP-	2.11	2.16	2.25	2.24	2.24	2.28	2.34	2.17	2.23	2.32
	ACM-	2.34	2.33	2.43	2.39	2.44	2.57	2.48	2.33	2.27	2.77

Table 3. Total Surface Acidic and Basic Groups of ACs

samples	basic functional group (mmol/g)			acidic functional group (mmol/g)		
	AC-	ACP-	ACM-	AC-	ACP-	ACM-
2/1-800-60	1.013 (±0.011)	1.031 (±0.012)	1.534 (±0.018)	0.114 (±0.014)	0.159 (±0.010)	0.252 (±0.027)
2/1-850-60	1.026 (±0.001)	1.099 (±0.009)	1.592 (±0.003)	0.138 (±0.025)	0.211 (±0.005)	0.257 (±0.005)
2/1-900-60	1.082 (±0.009)	1.134 (±0.005)	1.749 (±0.005)	0.164 (±0.005)	0.314 (±0.005)	0.324 (±0.020)
2/1-950-60	1.177 (±0.008)	1.211 (±0.019)	2.112 (±0.011)	0.163 (±0.014)	0.355 (±0.016)	0.357 (±0.020)
2/1-900-40	0.943 (±0.033)	1.138 (±0.004)	1.828 (±0.002)	0.164 (±0.001)	0.286 (±0.021)	0.294 (±0.007)
2/1-900-80	0.944 (±0.009)	1.113 (±0.011)	1.751 (±0.031)	0.146 (±0.016)	0.330 (±0.006)	0.341 (±0.009)
2/1-900-100	0.945 (±0.004)	1.090 (±0.01417)	1.715 (±0.02217)	0.123 (±0.007)	0.323 (±0.005)	0.314 (±0.014)
5/1-900-60	0.930 (±0.002)	0.912 (±0.008)	1.629 (±0.035)	0.092 (±0.002)	0.303 (±0.007)	0.226 (±0.004)
3/1-900-60	0.960 (±0.032)	1.081 (±0.003)	1.636 (±0.005)	0.121 (±0.012)	0.315 (±0.004)	0.245 (±0.008)
1/1-900-60	1.068 (±0.002)	1.226 (±0.033)	2.105 (±0.008)	0.176 (±0.013)	0.385 (±0.027)	0.351 (±0.007)

had a higher S_{BET} compared with that of AC when the activation temperature was 800 °C (340 m²/g), whereas the S_{BET} of ACM at a higher activation temperature (≥850 °C) was lower than that of AC prepared under the same condition. ACP showed a similar variation compared with that of ACM; its S_{BET} increased from 338 m²/g at 800 °C to 443 m²/g at 950 °C.

For each series of samples, the higher S_{BET} corresponded to the larger V_{tot}, both of them increased with the increasing activation temperature. AC, ACP, and ACM had the largest V_{tot} of 0.252, 0.248, and 0.272 m³/g, respectively, when the activation temperature was 950 °C. It should be noted that the pore structure of ACM was more developed, which had the biggest Vtot, even though its S_{BET} was relatively smaller than AC. Compared with the nonmodified AC, the V_{mic} of the modified ACP and ACM was less, and alternatively, they had a relatively higher V_{mes}. This variation is consistent with the change of S_{mes}. Therefore, it could be deduced that the blending of MnO_2 and pyrolusite is favorable for the mesoporous structure formation during steam activation, especially for MnO_2.

The comparison of nonmodified AC and blending-modified ACs showed that the blending of MnO_2 and pyrolusite was favorable for the S_{BET} at a relatively low activation temperature (800 °C), whereas the increase of activation temperature is more favorable for the nonmodified AC to have a bigger S_{BET}. The blending of MnO_2 and pyrolusite improved the formation of the mesoporous structure but debased the S_{BET} of samples to a certain extent under the same conditions.

2.2.3. Surface Functional Groups of ACs. Surface functional groups, another important parameter that affected the preparation of ACs, were quantified, and the results are listed in Table 3. The acidic and basic sites on the surface of AC were proportionate to the increment of activation temperature; they were increased from 0.1136 and 1.0126 mmol/g at 800 °C to 0.1631 and 1.1765 mmol/g at 950 °C, respectively. The surface functional groups of the metal-modified ACs were higher than the fresh AC, especially ACM. The surface basic sites of ACM were more than 50.0% higher than AC at 800 °C activation temperature (1.5336 mmol/g), and it dramatically increased to 2.1124 mmol/g when the activation temperature increased to 950 °C. The increase of acidic functional groups of the modified ACs was more significant; they were mostly doubled compared with that of AC. The difference of improvement between the acidic and basic functional groups means that different metal oxides that participated in activation performed different functions in the form of surface functional groups, and the higher temperature seems more favorable for the acidic functional group formation with the presence of transition metal oxide. It was reported that thermal treatments
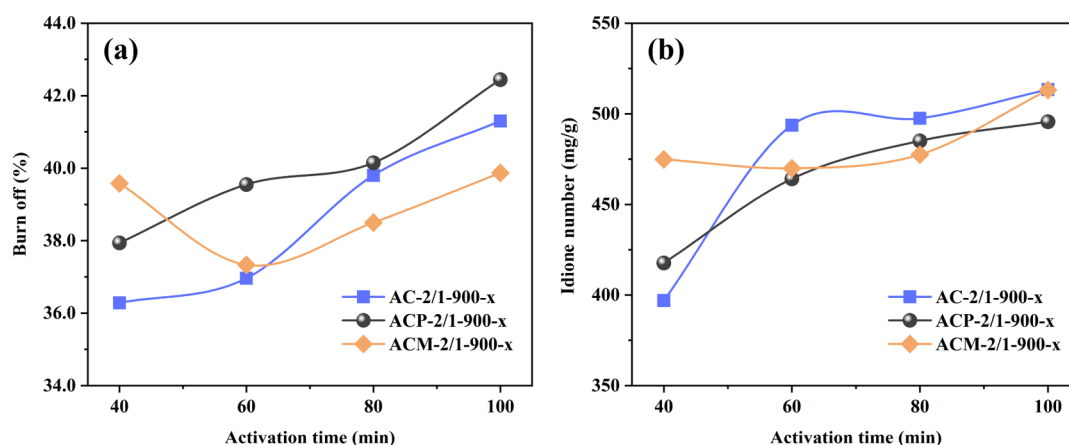
Figure 4. BO (a) and iodine number (b) of ACs prepared under different activation times.

have produced ACs with basic character;[37] the difference could be due to the addition of MnO_2 and pyrolusite, and the addition changed the direction of surface functional group formation. Previous investigations indicated that the Fe species inhibited the production of functional groups, which might explain why the surface acidic and basic functional groups of ACM were greater than those of ACP in the same situation.[38]

2.3. Influences of Activation Time. *2.3.1. BO and Iodine Number of ACs.* Figure 4 shows the BO and iodine number of the samples prepared under different activation times. The BO of all samples was proportional to the activation time, except the BO of ACM-2/1-900-40. The BO of AC grew slowly from 36.28 to 36.96% when the activation time ranged from 40 to 60 min, but it increased rapidly when the activation time was longer than 60 min (Figure 4a). The difference in BO between ACP and AC was gradually diminished as the activation time increases, whereas the difference between ACM and AC gradually advanced. When the activation time was greater than 60 min, the order of BO from high to low followed the order ACP > AC > ACM at the same activation time. For the clearly higher BO of the ACM-2/1-900-40 sample, it should be attributed to the higher water steam supply. This will be discussed later with the influences of M_C/M_{H_2O}. As shown in Figure 4b, the change in BO was reflected on the iodine number of samples. The iodine number of AC was 397 mg/g at 40 min activation time and increased to 513 mg/g when the activation time was prolonged to 60 min. Further increase of activation time had a limited effect on the iodine number of AC, even though its BO became greater. The blending of pyrolusite showed almost an adverse effect on the iodine number, three of four ACP prepared at different activation times had lower iodine numbers than AC prepared at the same activation time. On the other hand, MnO_2 blending made ACM have a greatly higher iodine adsorption capacity at 40 min activation time, whereas the iodine number of ACM prepared at a longer activation time was smaller. The comparison of the BO and the iodine number of three series of samples revealed that the blending modification made a great difference in the iodine number of ACs prepared with a shorter activation time, but the influences were indistinctive when the activation period was more than 60 min.

2.3.2. Textual Property of ACs. As is shown in Figure 5, the N_2 adsorption−desorption isotherms of ACs prepared under different activation times have similar characteristics. More than 70% of the N_2 adsorption capacity happened at a low-
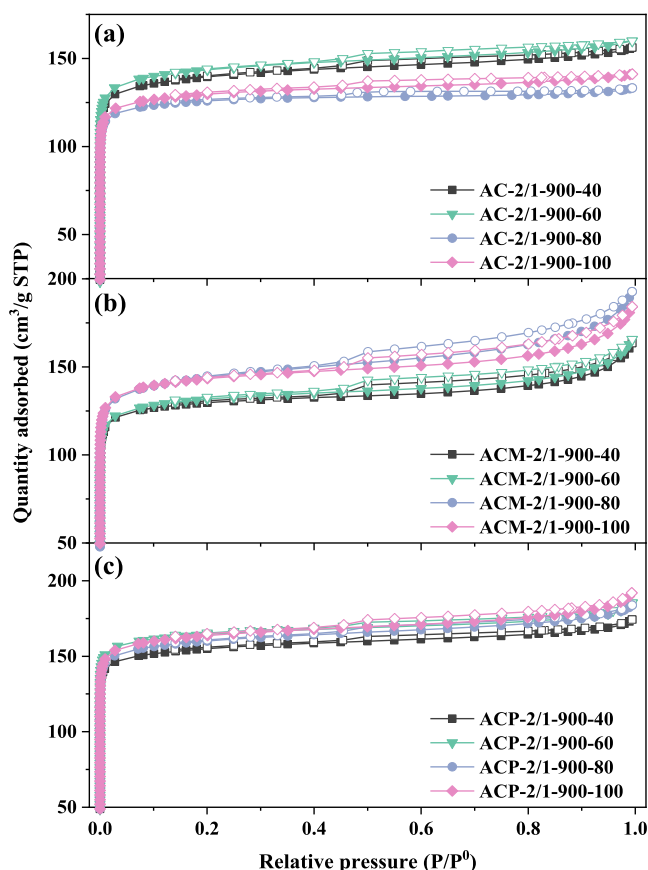

Figure 5. N_2 adsorption−desorption isotherms of ACs prepared under different activation times: (a) AC-, (b) ACM-, and (c) ACP-.

pressure range ($P/P^0 < 0.1$). The mesoporous structures of ACP and ACM were more developed than those of AC, especially ACM, because of the higher N_2 adsorption capacity in the high P/P^0 range (>0.9) and the clearer hysteresis loops.[39,40]

The S_{BET} of AC showed a convex parabolic change, which had the highest S_{BET} (459 m^2/g) at 60 min activation time (Table 2), even though the BO of samples linearly increased with increasing activation time. For the ACP series sample, the activation time affected slightly on the S_{BET}, less than 5% change of S_{BET} performed when the activation time was 60 min or more. The S_{BET} of ACM showed a very close variation to
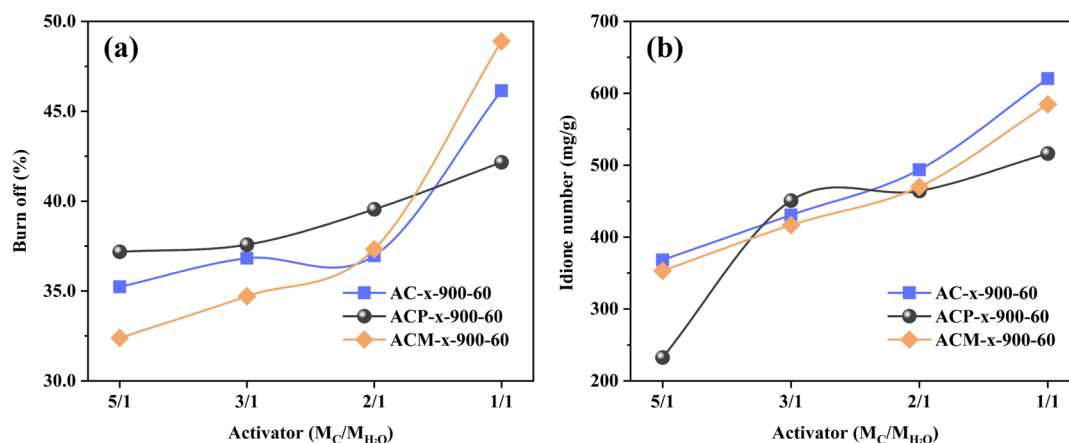
**Figure 6.** BO (a) and iodine number (b) of ACs prepared under different activators (M_C/M_{H_2O}).

ACP, but ACM had a higher S_{BET} than AC and ACP, which is similar to the influences of the activation temperature. The V_{tot} values of ACP and ACM were both higher than that of AC at the same activation time, even though the S_{BET} of ACM was lower than AC at 40 and 60 min. The blending of metal oxides changed the effect of activation time on the pore structure formation of ACs; the V_{mic} and V_{mes} of ACM and ACP were progressively higher with the longer activation time, which is opposite to the reduction of AC. Moreover, the change of activation time showed a greater effect on the V_{mes} of metal-oxide-blended ACs than the activation temperature, and the differences of V_{mes} of ACM and ACP prepared at different activation times were clearly bigger. Therefore, an appropriate increase in the activation time can effectively improve the mesoporous structure of the metal-oxide-blended ACs, but the fresh AC needs a relative shorter activation time to retain more V_{mes}.

2.3.3. Surface Functional Groups of ACs. As is shown in Table 3, the surface acidic and basic functional groups of AC both first increased and then linearly reduced with the increase of activation time, and AC-2/1-900-60 had the highest content of acidic and basic functional groups of 0.1635 ($\pm$0.0002) and 1.0817 ($\pm$0.0081) mmol/g, respectively. ACP and ACM had more surface functional groups, even though their basic functional groups were gradually reduced with increased activation time. When the activation time was 40 min, ACP and ACM had the largest content of basic functional groups, which were 1.1384 ($\pm$0.0041) and 1.8277 ($\pm$0.0017) mmol/g, respectively. The change of surface acidic sites of ACP and ACM was similar to that of AC, and when the activation time was 80 min, ACP and ACM had the highest content of acidic functional groups at 0.3297 ($\pm$0.0060) and 0.3405 ($\pm$0.0087) mmol/g, respectively. The changes of surface functional groups of three series of samples indicate that the blended MnO_2 and pyrolusite enhanced and accelerated the formation of surface functional groups under the same preparation condition. There is a reduction of functional groups with the increase of activation time because of the decomposition at a high temperature. Furthermore, the consistent content of water steam supplied caused different steam concentrations during the activation process. The influence of steam concentration on the physicochemical properties of ACs will be discussed later.

2.4. Influences of M_C/M_{H_2O}. *2.4.1. BO and Iodine Number of ACs.* Figure 6 depicts the influences of the amount of steam supplied (M_C/M_{H_2O}) on the BO and iodine number of the prepared ACs. The BO of AC changed inconspicuously when the M_C/M_{H_2O} decreased from 5/1 to 2/1, only 1.73% more carbon loss of AC-2/1-900-60 (36.96%) compared with AC-5/1-900-60 (35.23%) (Figure 6a). When the M_C/M_{H_2O} was lower to 1/1, the BO greatly increased almost 10−46.14%. The blending of pyrolusite diminished the effect of M_C/M_{H_2O} on the BO of samples; the whole change of the BO of ACP was only 4.98%. ACP had a relatively greater BO than AC when the M_C/M_{H_2O} decreased from 5/1 to 2/1, whereas the BO of ACP prepared at M_C/M_{H_2O} = 1/1 was significantly lower than AC. Although the blended MnO_2 brings some difference, the BO of ACM showed a similar change with AC with the change of water steam. The blended MnO_2 inhibited the mass loss under high M_C/M_{H_2O} (5/1−3/1) condition, but the BO of ACM will be bigger if the water steam supply is too much. The BO of ACM-5/1-900-60 (32.39%) and ACM-3/1-900-60 (34.71%) were less than 35%, but the BO of ACM-1/1-900-60 increased 2.75−48.89% compared with that of AC prepared at the same conditions. This indicates that the flow rate of water steam affects the BO greatly, and the extremely higher BO of ACM-2/1-900-40 could be explained. Figure 6b shows the iodine number of samples. AC and ACM had a very close number of iodine number, indicating that MnO_2 blending affects the surface area of samples weakly, even though the BO of ACM was clearly changed. The blending of pyrolusite changed the adsorption property of ACs greatly. ACP-5/1-900-60 had the highest BO compared with AC and ACM when the M_C/M_{H_2O} = 5/1, whereas its iodine number was the lowest. This could be attributed to the non-metallic ash introduced by pyrolusite blending;[28] it might be to reduce the mass loss at a smaller M_C/M_{H_2O} (ACP-1/1-900-60).

2.4.2. Textual Property of ACs. The N_2 adsorption−desorption isotherms of ACs prepared under different M_C/M_{H_2O} are shown in Figure 7. Similar to the effect of activation temperature, the N_2 isotherms and hypothesis of samples prepared at different M_C/M_{H_2O} were almost still characteristic type I, except ACM-1/1-900-60. The more water steam supplied for activation, the larger N_2 adsorption capacity of samples obtained, particularly in the high relative pressure range, which corresponded to the mesoporous structure. The hysteresis of the ACM-1/1-900-60 sample is evolving to H3
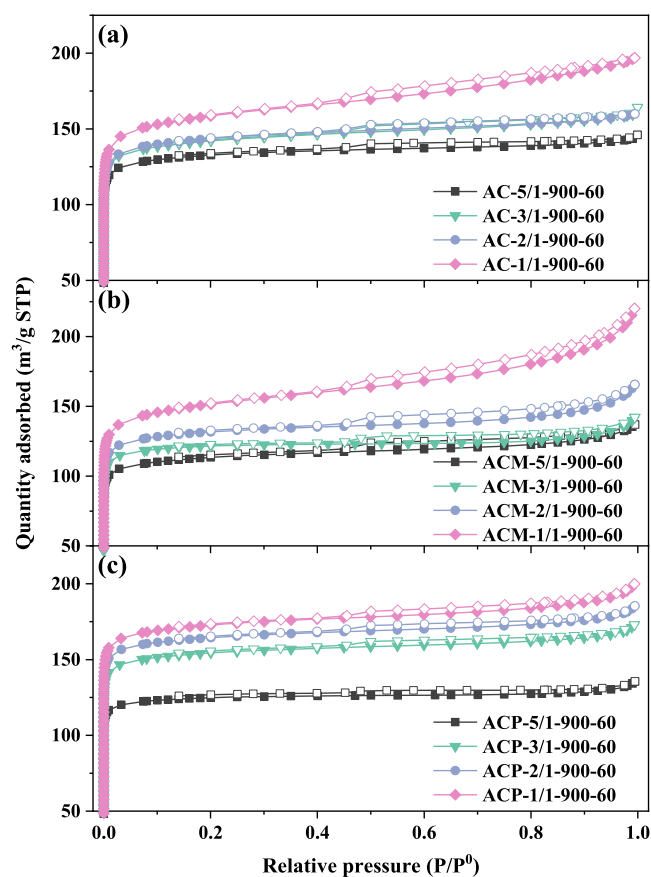
Figure 7. N_2 adsorption−desorption isotherms of ACs prepared under different M_C/M_{H_2O}: (a) AC-, (b) ACM-, and (c) ACP-.

type, indicating that more slit-shaped pores with a bigger pore diameter are formed.[36] As is shown in Table 2, S_{BET} of AC and ACM increased slowly with the reduction of M_C/M_{H_2O} when M_C/M_{H_2O} was bigger than 2/1; they were 423 and 363 m^2/g at M_C/M_{H_2O} = 5/1 and increased to 459 and 421 m^2/g when the M_C/M_{H_2O} was 2/1, respectively. When M_C/M_{H_2O} further reduced to 1/1, S_{BET} of AC and ACM further increased by 42 and 69 m^2/g to 511 and 490 m^2/g, respectively. Although the BO increased feebly when M_C/M_{H_2O} decreased from 5/1 to 3/1, their S_{BET} increased rapidly from 285 to 385 m^2/g and then their S_{BET} increased very slowly with the continuous decrease of M_C/M_{H_2O}. Based on the comparison of V_{mic} and V_{mes} of samples, we know that the effect of blended metal oxide on the mesoporous structure of ACs is stronger than the effect of water steam, and different metal oxides or mixtures have significant differences in their effects. The blended MnO_2 further promoted the V_{mes} formation of ACM, whereas the pyrolusite promoted inhibition. The differences of textual properties of ACs prepared at different M_C/M_{H_2O} show that ACs can obtain a better pore structure with a relatively small M_C/M_{H_2O}, and M_C/M_{H_2O} has limited effect on the pore structure of ACs when it was bigger than 2/1. However, ACP and ACM need more water steam to obtain the same pore structure, and the increased water steam during activation is more favorable for the mesoporous structure formation.

2.4.3. Surface Functional Groups of ACs. The surface functional groups of the AC samples prepared under different

M_C/M_{H_2O} values are listed in Table 3. The content of basic functional groups of AC first increased with the reduction of M_C/M_{H_2O}, AC had the highest basic functional groups of 1.0817 mmol/g when the M_C/M_{H_2O} was 2/1, and then it was relatively stable when the M_C/M_{H_2O} was further reduced. On the other hand, the more water steam supplied in activation, the more surface acidic functional groups of the AC products. The number of acidic functional groups of AC-1/1-900-60 almost doubled to 0.1761 mmol/g as compared with AC-5/1-900-60 (0.0919 mmol/g). After being blended with pyrolusite, the basic and acidic functional groups of ACP showed a similar change with the vibration of M_C/M_{H_2O}, even though their functional groups were clearly higher than those of AC. The blending of MnO_2 showed some difference with pyrolusite. It was found that the basic functional groups of AC showed a linear increase with the decrease of M_C/M_{H_2O}, and it was more than 60 and 55% higher than that of AC and ACP at the same M_C/M_{H_2O}. The acidic functional groups of ACM were slightly less than that of ACP, but they were almost double as compared to AC. Based on the abovementioned results, it can be said that an appropriate increase in the amount of water steam for activation can effectively increase the content of acidic−basic functional groups of the surface of the AC product. The blending of MnO_2 or pyrolusite works is more for the functional group formation, and MnO_2 is more favorable for the formation of basic functional groups.

2.5. Desulfurization Performance of the Prepared ACs. The low-temperature desulfurization performance of the prepared AC, ACM, and ACP is shown in Figure 8. It can be seen that the higher the activation temperature, longer the activation time and bigger the water steam supplied for the preparation of ACs, and higher the sulfur capacity of the obtained ACs. The sulfur capacities of ACP and ACM were in the range of 47.9−208.9 and 119.4−205.9 mg/g, respectively. Both of them had much higher sulfur capacity than the fresh AC at the same activation condition, except ACP-5/1-900-60 (49.0 mg/g). The comparison of ACM and ACP indicated that the ACM series samples performed better desulfurization activity than ACP when they were prepared at the same conditions. This result is different from Fan's previous work[28] and it might be attributed to the different loading amount of additives. Also, pyrolusite that we used is also different. The change of sulfur capacity at different activation times for unmodified AC suggests that the desulfurization capability is more dependent on its surface functional groups, and the reduced surface acidity (lower acidic functional groups) is favorable for the acid gas SO_2 adsorption on the surface.[41] The key explanations for the increased desulfurization performance of the modified ACP and ACM were the alteration of surface oxygen-containing functional groups and the catalytic activity of transition metal components; this has been reported elsewhere.[42,43] ACM and ACP samples possessed more basic functional groups to increase SO_2 adsorption, and the more surface oxygen and metal oxides/elements introduced results in quicker oxidation of the adsorbed SO_2. Moreover, the blended transition metal of ACM and ACP can promote the electron transfer in the process of SO_2 oxidation, which can enhance the chemical reaction; in other words, it played a catalytic role. All of these show that ACP and ACM have a higher sulfur capacity.[42,44]
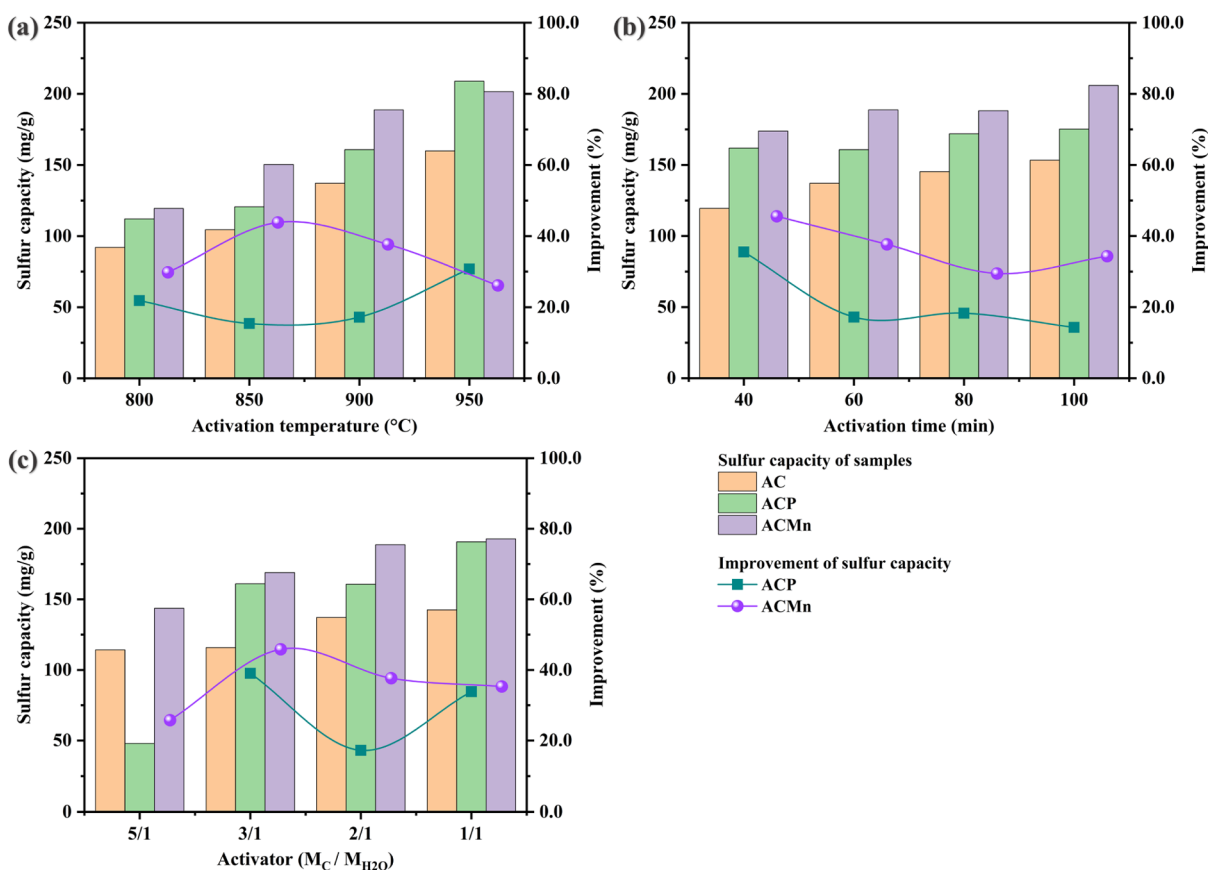
Figure 8. Sulfur capacity of the prepared ACs: (a) effect of the activation temperature, (b) effect of the activation time, and (c) effect of M_C/M_{H_2O} (The inlet SO_2 was 3000 ppm, space velocity was 600 h^{-1}, oxygen was 8%, flue gas humidity was 10%, and the working temperature was 80 °C).

Comparing the effect of the activation temperature, activation time, and water steam supply on the desulfurization performance of ACs revealed that the activation temperature had the most significant impact on the SO_2 removal activity, followed by the water vapor amount, and the activation time has the smallest influence. The blending of pyrolusite and MnO_2 further reduced the function of activation time on the desulfurization process, but the effect of water steam became clearer. Based on the abovementioned information, we can say that 4 wt % blending of MnO_2 is better than 4 wt % pyrolusite blending for SO_2 removal. The optimum preparation conditions of ACs for SO_2 removal are varied from the additive blended.

3. CONCLUSIONS

In this study, the preparation of MnO_2 and pyrolusite blending-modified activated cokes was comparatively studied. The results reveal that the influences of activation temperature, time, and water vapor on the physicochemical properties of blending-modified ACs are significantly different from those of the conventional ACs. S_{BET} of ACM and ACP was decreased to varying degrees in relation to AC at higher activation temperatures, whereas both of them had a better pore structure at lower activation temperatures. The blended MnO_2 and pyrolusite overcame the adverse effect of long activation time, and the pore structure of ACM and ACP showed a continuous improvement with the increase of activation time. ACM and ACP required more water steam supply to obtain the same pore structure of AC. The blending

modification greatly improved the mesoporous structure generation of ACM and ACP at the same preparation conditions. After being blended with metal oxides, the surface acidic and basic functional groups of ACP and ACM were significantly increased; especially for ACM, its functional groups were almost double compared to AC. Comparison of ACM and ACP shows that the influences of different metal oxides on the pore structure and surface functional groups were different, and MnO_2 is better for the formation of a more developed porous structure and more abundant surface functional groups of AC than iron oxides. Because of the promoted surface adsorption of SO_2 and O_2 molecules and surface oxidation by the surface functional groups and the catalytic activity of metal oxides, respectively, the desulfurization activity of ACP and ACM was significantly improved. The sulfur capacities of ACP and ACM were in the range of 47.9–208.9 and 119.4–205.9 mg/g, respectively, clearly higher than the nonmodified AC.

4. EXPERIMENTAL SECTION

4.1. Preparation of ACs. The proximate analysis of the two coals and the binder coal tar used for AC preparation is shown in Table 4. All the AC samples prepared in this study were based on the previous coal blending study, in which the mass ratio of bituminous coal to 1/3 coking coal was 3/1; the coal tar used was 40 ± 1%. The detailed preparation process of ACs was described in detail in the previous study,[38] and the prepared AC samples were 3 mm in diameter, columnar, and granular. For the modified AC, pyrolusite (200 mesh powder),

Table 4. Main Ingredients of the Raw Materials and Main Binder (wt %)

samples	C	H	O	N	S
bituminous coal	73.78	9.69	14.10	2.29	0.14
1/3 coking coal	74.23	4.83	17.39	2.08	1.47
coal tar	80.08	3.91	14.55	1.20	0.26

which majorly consists of Mn (39.40%), Fe (6.27%), Si (4.10%), Ca (1.30%), Ni (0.07%), Cu (0.06%), and Co (0.06%), or the 200 mesh MnO_2 powder (AR, 90%, Chron Chemicals), was mixed with the coal powder directly at the weight ratio of 4 wt % before the coal tar was added.

The carbonization and activation processes were run based on the following steps: the granular carbon was first heated to 600 °C and made to undergo carbonization for 60 min. After that, the reactor was continually heated to the activation temperature (800, 850, 900, and 950 °C) and physically activated using water steam (M_C/M_{H_2O} = 5/1, 3/1, 2/1, and 1/1) for a certain time (40, 60, 80, and 100 min). The whole heating process was run in a N_2 atmosphere except the water steam activation; the heating rate was 5 °C/min. When the activation was down, heating was turned off and the water steam was replaced by N_2 flow and naturally cooled to room temperature. In addition to the parameters discussed, the activation temperature, activation time, and M_C/M_{H_2O} were kept at 900 °C, 60 min, and M_C/M_{H_2O} = 2/1, respectively. The nomenclature of each coke sample consists of activated coke (ACX, X is the corresponding modifier, P represents pyrolusite, and M represents MnO_2), the content of activator a (M_C/M_{H_2O}), the activation temperature (T_A), and the activation time (t) in minutes. For example, pyrolusite-modified AC, which was prepared at an activation temperature of 900 °C with a M_C/M_{H_2O} = 3/1 for 60 min, will be named as ACP-3/1-900-60.

4.2. Characterization. The BO of samples was defined as the ratio of mass loss during the carbonization and activation processes, which was calculated using eq 31

$$\text{burn off(\%)} = \left(\frac{m_1 - m_2}{m_1}\right) \times 100\% \tag{31}$$

where m_1 is the total mass of granular carbon before activation and m_2 is the total mass of activated coke after activation (g).

The iodine number is defined in terms of the milligrams of iodine (I_2) adsorbed by 1 g of AC, which gives information on the surface area contributed by pores larger than 1 nm.[45] In this study, the iodine number of the ACs was determined according to the Chinese National Standards—Test method for granular activated carbon from coal—Determination of iodine number (GB/T 7702.7-2008).[46]

N_2 adsorption—desorption isotherms of ACs were measured using an automatic sorptometer (Micromeritics, ASAP 2460, USA) at −196 °C. Prior to measurements, the samples were degassed at 250 °C for 8 h under vacuum. The specific surface areas of ACs were calculated using the Brunauer−Emmett−Teller (BET) equation, assuming the area of the nitrogen molecule to be 0.162 nm². The total pore volume was estimated as the liquid volume of N_2 adsorbed at a relative pressure of 0.995. The micropore volume and micropore surface area were obtained using the t-plot theory. The

mesopore volume was calculated by the Barret−Joyner−Halenda (desorption) model.

XRD analysis of the samples was carried out on a PANalytical-Empyrean diffractometer equipped with a Cu Kα radiation (λ = 1.5406 Å) in the 2θ range of 10 to 80° at 40 kV and 30 mA.

The determination of surface acidic and basic groups of the prepared ACs was performed using NaOH or HCl uptake methods. 25 mL of 0.05 N NaOH or 0.05 N HCl was added to 200 mg of coke in several 50 mL vials. The bottles were sealed and allowed to equilibrate for 24 h in an oscillator at room temperature. At the end of the equilibration period, 10 mL of the solution was titrated with 0.05 N of either NaOH or HCl solution. The total acidic groups were calculated as the difference in the amount of acid required to titrate the blank to a pH of 4.5 and the amount of acid required to titrate the sample to the same end point. Meanwhile, the total basicity was calculated as the difference in the amount of acid required to titrate the blank to a pH of 11.5 and the amount of acid required to titrate the sample to the same end point.

4.3. Desulfurization Test. The performance of flue gas desulfurization was carried out in a self-designed and assembled laboratory fixed-bed reactor. The reactor was a 21 mm diameter glass tube and packed with 100 mm height of the AC (about 20 ± 2 g of samples), which was varied with different additives and preparation conditions. The desulfurization temperature was 80 °C, the space velocity was 600 h^{-1}, and the compositions of simulated flue gas were 3000 ppm of SO_2, 10% of O_2, 10% of water vapor, and N_2 as the balance gas. The inlet and outlet SO_2 were continuously monitored online by a flue gas analyzer (Gasboard 3000, China). The desulfurization test was terminated when the outlet SO_2 reached 10% of the inlet concentration (300 ppm), and the sulfur capacity was calculated based on the breakthrough curve using eq 32

$$\text{sulfur capacity(mg/g)}$$
$$= \frac{\sum_{i=1}^{n} q \times (c_0 - c_i) \times t \times M \times 10^{-6}}{22.4 \times m} \tag{32}$$

where q is the total flue gas flow (mL/min), c_0 is the inlet SO_2 concentration (ppm), c_i is the outlet SO_2 concentration at the i-th sampling (ppm), t is the sampling interval (5 min), n is the total time of sampling, m is the mass of samples (g), and M is the molar mass of SO_2.

■ AUTHOR INFORMATION

Corresponding Author

Lin Yang − *College of Architecture and Environment, Sichuan University, Chengdu, Sichuan 610065, China; National Engineering Research Center for Flue Gas Desulfurization, Sichuan University, Chengdu, Sichuan 610065, China; National Engineering Laboratory for Clean Technology of Leather Manufacture, Sichuan University, Chengdu, Sichuan 610065, China;* ⊙ orcid.org/0000-0002-3367-244X; Email: evanlinyang@sina.com

Authors

Wenjie Liao − *College of Architecture and Environment, Sichuan University, Chengdu, Sichuan 610065, China*

Xiaomi Meng − *College of Architecture and Environment, Sichuan University, Chengdu, Sichuan 610065, China*

Lu Yao − *College of Architecture and Environment, Sichuan University, Chengdu, Sichuan 610065, China; National Engineering Research Center for Flue Gas Desulfurization, Sichuan University, Chengdu, Sichuan 610065, China;* ⊙ orcid.org/0000-0003-2743-758X

Wenju Jiang − *College of Architecture and Environment, Sichuan University, Chengdu, Sichuan 610065, China; National Engineering Research Center for Flue Gas Desulfurization, Sichuan University, Chengdu, Sichuan 610065, China;* ⊙ orcid.org/0000-0003-1327-7159

Complete contact information is available at:
https://pubs.acs.org/10.1021/acsomega.1c03280

Author Contributions

The manuscript was written through contributions of all authors. All authors have given approval to the final version of the manuscript.

Funding

Notes

The authors declare no competing financial interest.

■ REFERENCES

(1) Yang, L.; Wang, P.; Yao, L.; Meng, X.; Jia, C. Q.; Jiang, X.; Jiang, W. Copper doping promotion on Ce/CAC-CNT catalysts with high sulfur dioxide tolerance for low-temperature NH₃−SCR. *ACS Sustain. Chem. Eng.* **2021**, *9*, 987−997.

(2) Yao, L.; Yang, L.; Jiang, W.; Jiang, X. Removal of SO₂ from flue gas on a copper modified activated coke prepared by a novel one-step carbonization activation blending method. *Ind. Eng. Chem. Res.* **2019**, *58*, 15693−15700.

(3) Tian, W.; Zhang, H.; Duan, X.; Sun, H.; Tade, M. O.; Ang, H. M.; Wang, S. Nitrogen- and sulfur-codoped hierarchically porous carbon for adsorptive and oxidative removal of pharmaceutical contaminants. *ACS Appl. Mater. Interfaces* **2016**, *8*, 7184−7193.

(4) Tong, K.; Lin, A.; Ji, G.; Wang, D.; Wang, X. The effects of adsorbing organic pollutants from super heavy oil wastewater by lignite activated coke. *J. Hazard. Mater.* **2016**, *308*, 113−119.

(5) Chen, P.; Wang, L.-K.; Wang, G.; Gao, M.-R.; Ge, J.; Yuan, W.-J.; Shen, Y.-H.; Xie, A.-J.; Yu, S.-H. Nitrogen-doped nanoporous carbon nanosheets derived from plant biomass: an efficient catalyst for oxygen reduction reaction. *Energy Environ. Sci.* **2014**, *7*, 4095−4103.

(6) Long, X.-L.; Xin, Z.-L.; Wang, H.-X.; Xiao, W.-D.; Yuan, W.-K. Simultaneous removal of NO and SO₂ with hexamminecobalt(II) solution coupled with the hexamminecobalt(II) regeneration catalyzed by activated carbon. *Appl. Catal., B* **2004**, *54*, 25−32.

(7) Tao, S.; Li, C.; Fan, X.; Zeng, G.; Lu, P.; Zhang, X.; Wen, Q.; Zhao, W.; Luo, D.; Fan, C. Activated coke impregnated with cerium chloride used for elemental mercury removal from simulated flue gas. *Chem. Eng. J.* **2012**, *210*, 547−556.

(8) Olson, D. G.; Tsuji, K.; Shiraishi, I. The reduction of gas phase air toxics from combustion and incineration sources using the MET−Mitsui−BF activated coke process. *Fuel Process. Technol.* **2000**, *65−66*, 393−405.

(9) Li, J.; Kobayashi, N.; Hu, Y. The activated coke preparation for SO₂ adsorption by using flue gas from coal power plant. *Chem. Eng. Process.* **2008**, *47*, 118−127.

(10) Liu, L.; Wang, B.; Yao, X.; Yang, L.; Jiang, W.; Jiang, X. Highly efficient MnOx/biochar catalysts obtained by air oxidation for low-temperature NH₃-SCR of NO. *Fuel* **2021**, *283*, 119336.

(11) Shafeeyan, M. S.; Daud, W. M. A. W.; Houshmand, A.; Shamiri, A. A review on surface modification of activated carbon for carbon dioxide adsorption. *J. Anal. Appl. Pyrol.* **2010**, *89*, 143−151.

(12) Jin, Z.; Wang, B.; Ma, L.; Fu, P.; Xie, L.; Jiang, X.; Jiang, W. Air pre-oxidation induced high yield N-doped porous biochar for improving toluene adsorption. *Chem. Eng. J.* **2020**, *385*, 123843.

(13) Yao, L.; Liu, Q.; Mossin, S.; Nielsen, D.; Kong, M.; Jiang, L.; Yang, J.; Ren, S.; Wen, J. Promotional effects of nitrogen doping on catalytic performance over manganese-containing semi-coke catalysts for the NH₃-SCR at low temperatures. *J. Hazard. Mater.* **2020**, *387*, 121704.

(14) Liu, H.; Li, G.; Hu, C. Selective ring C-H bonds activation of toluene over Fe/activated carbon catalyst. *J. Mol. Catal. A: Chem.* **2013**, *377*, 143−153.

(15) Fang, H.-b.; Zhao, J.-t.; Fang, Y.-t.; Huang, J.-j.; Wang, Y. Selective oxidation of hydrogen sulfide to sulfur over activated carbon-supported metal oxides. *Fuel* **2013**, *108*, 143−148.

(16) Mei, Z.; Shen, Z.; Zhao, Q.; Wang, W.; Zhang, Y. Removal and recovery of gas-phase element mercury by metal oxide-loaded activated carbon. *J. Hazard. Mater.* **2008**, *152*, 721−729.

(17) Barroso-Bogeat, A.; Alexandre-Franco, M.; Fernández-González, C.; Gómez-Serrano, V. Preparation of activated carbon-metal oxide hybrid catalysts: textural characterization. *Fuel Process. Technol.* **2014**, *126*, 95−103.

(18) Buczek, B.; Ziętek, S.; Świątkowski, A. Radial heterogeneity of impregnated active carbon particles. *Langmuir* **1997**, *13*, 1342−1344.

(19) Wang, J. C.; Liu, Q. Y.; Liu, Z. Y.; Huang, Z. G. Heterogeneity of V₂O₅ supported cylindrical activated coke used for SO₂ removal from flue gas. *Chem. Eng. Technol.* **2008**, *31*, 1056−1061.

(20) Kaluža, L.; Zdražil, M. Carbon-supported Mo catalysts prepared by a new impregnation method using a MoO₃/water slurry: saturated loading, hydrodesulfurization activity and promotion by Co. *Carbon* **2001**, *39*, 2023−2034.

(21) Belhachemi, M.; Rios, R. V. R. A.; Addoun, F.; Silvestre-Albero, J.; Sepúlveda-Escribano, A.; Rodríguez-Reinoso, F. Preparation of activated carbon from date pits: Effect of the activation agent and liquid phase oxidation. *J. Anal. Appl. Pyrol.* **2009**, *86*, 168−172.

(22) Yang, L.; Huang, T.; Jiang, X.; Li, J.; Jiang, W. The effects of metal oxide blended activated coke on flue gas desulphurization. *RSC Adv.* **2016**, *6*, 55135−55143.

(23) Sawant, S. Y.; Munusamy, K.; Somani, R. S.; John, M.; Newalkar, B. L.; Bajaj, H. C. Precursor suitability and pilot scale production of super activated carbon for greenhouse gas adsorption and fuel gas storage. *Chem. Eng. J.* **2017**, *315*, 415−425.

(24) Stavropoulos, G. G. Precursor materials suitability for super activated carbons production. *Fuel Process. Technol.* **2005**, *86*, 1165−1173.

(25) Fan, L.; Jiang, X.; Jiang, W.; Guo, J.; Chen, J. Physicochemical properties and desulfurization activities of metal oxide/biomass-based activated carbons prepared by blending method. *Adsorption* **2014**, *20*, 747−756.

(26) Li, J.; Kobayashi, N.; Hu, Y. Performance of V₂O₅/AC activated with the flue gas on SO₂ removal. *J. Environ. Eng.* **2009**, *4*, 176−187.

(27) Guo, J.-X.; Fan, L.; Peng, J.-F.; Chen, J.; Yin, H.-Q.; Jiang, W.-J. Desulfurization activity of metal oxides blended into walnut shell based activated carbons. *J. Chem. Technol. Biotechnol.* **2014**, *89*, 1565−1575.

(28) Fan, L.; Chen, J.; Guo, J.; Jiang, X.; Jiang, W. Influence of manganese, iron and pyrolusite blending on the physiochemical properties and desulfurization activities of activated carbons from walnut shell. *J. Anal. Appl. Pyrol.* **2013**, *104*, 353−360.

(29) Wang, P.; Jiang, X.; Zhang, C.; Zhou, Q.; Li, J.; Jiang, W. Desulfurization and regeneration performance of titanium ore modified activated coke. *Energy Fuel* **2017**, *31*, 5266−5274.

(30) Yang, L.; Huang, T.; Jiang, X.; Jiang, W. Effect of steam and CO₂ activation on characteristics and desulfurization performance of pyrolusite modified activated carbon. *Adsorption* **2016**, *22*, 1099−1107.

(31) Lin, S.-Y.; Suzuki, Y.; Hatano, H.; Harada, M. Hydrogen production from hydrocarbon by integration of water–carbon reaction and carbon dioxide removal (HyPr–RING Method). *Energy Fuel.* **2001**, *15*, 339–343.

(32) Feng, Y.-l.; Cai, Z.-l.; Li, H.-r.; Du, Z.-w.; Liu, X.-w. Fluidized roasting reduction kinetics of low-grade pyrolusite coupling with pretreatment of stone coal. *Int. J. Miner., Metall. Mater.* **2013**, *20*, 221–227.

(33) Yang, L.; Jiang, X.; Yang, Z.-S.; Jiang, W.-J. Effect of $MnSO_4$ on the removal of SO_2 by manganese-modified activated coke. *Ind. Eng. Chem. Res.* **2015**, *54*, 1689–1696.

(34) Lee, Y.-W.; Park, J.-W.; Choung, J.-H.; Choi, D.-K. Adsorption characteristics of SO_2 on activated carbon prepared from coconut shell with potassium hydroxide activation. *Environ. Sci. Technol.* **2002**, *36*, 1086–1092.

(35) Lowell, S.; Shields, J. E.; Thomas, M. A.; Thommes, M. *Characterization of Porous Solids and Powders: Surface Area, Pore Size and Density*; Springer: Netherlands, 2012; Vol. *16*.

(36) Sing, K. S. W.; Everett, D. H.; Haul, R. A. W.; Moscou, L.; Pierotti, R. A.; Rouquerol, J.; Siemieniewska, T. Reporting physisorption data for gas/solid systems with special reference to the determination of surface area and porosity (Recommendations 1984). *Pure Appl. Chem.* **1985**, *57*, 603–619.

(37) Chingombe, P.; Saha, B.; Wakeman, R. J. Surface modification and characterisation of a coal-based activated carbon. *Carbon* **2005**, *43*, 3132–3143.

(38) Yang, L.; Jiang, X.; Jiang, W.; Wang, P.; Jin, Y. Cyclic regeneration of pyrolusite-modified activated coke by blending method for flue gas desulfurization. *Energy Fuel.* **2017**, *31*, 4556–4564.

(39) Wang, X.; Song, J.; Huang, J.; Zhang, J.; Wang, X.; Ma, R.; Wang, J.; Zhao, J. Activated carbon-based magnetic TiO_2 photocatalyst codoped with iodine and nitrogen for organic pollution degradation. *Appl. Surf. Sci.* **2016**, *390*, 190–201.

(40) Ahmad, A.; Loh, M.; Aziz, J. Preparation and characterization of activated carbon from oil palm wood and its evaluation on methylene blue adsorption. *Dyes Pigments* **2007**, *75*, 263–272.

(41) Moreno-Castilla, C.; Maldonado-Hódar, F. J.; Pérez-Cadenas, A. F. Physicochemical surface properties of Fe, Co, Ni, and Cu-doped monolithic organic aerogels. *Langmuir* **2003**, *19*, 5650–5655.

(42) Gao, X.; Liu, S.; Zhang, Y.; Luo, Z.; Cen, K. Physicochemical properties of metal-doped activated carbons and relationship with their performance in the removal of SO_2 and NO. *J. Hazard. Mater.* **2011**, *188*, 58–66.

(43) Fang, N.-J.; Guo, J.-X.; Shu, S.; Li, J.-J.; Chu, Y.-H. Influence of textures, oxygen-containing functional groups and metal species on SO_2 and NO removal over Ce-Mn/NAC. *Fuel* **2017**, *202*, 328–337.

(44) Guo, Y.; Du, E. The effects of thermal regeneration conditions and inorganic compounds on the characteristics of activated carbon used in power plant. *Energy Procedia* **2012**, *17*, 444–449.

(45) Hu, Z.; Srinivasan, M. P. Mesoporous high-surface-area activated carbon. *Microporous Mesoporous Mater.* **2001**, *43*, 267–275.

(46) General administration of quality supervision inspection and quarantine of the People's Republic of China; standardization administration of the People's Republic of China, test method for granular activated carbon from coal—Determination of iodine number. In China, 2008; Vol. GB/T 7702.7-2008.